



# Multiple treatments with liposomal doxorubicin and ultrasound-induced disruption of blood–tumor and blood–brain barriers improve outcomes in a rat glioma model<sup>☆</sup>

Muna Aryal<sup>a,b,\*</sup>, Natalia Vykhodtseva<sup>b</sup>, Yong-Zhi Zhang<sup>b</sup>, Juyoung Park<sup>b</sup>, Nathan McDannold<sup>b</sup>

<sup>a</sup> Department of Physics, Boston College, Chestnut Hill, USA

<sup>b</sup> Department of Radiology, Brigham & Women's Hospital, Harvard Medical School, Boston, USA

## ARTICLE INFO

### Article history:

Received 2 January 2013

Accepted 10 April 2013

Available online 18 April 2013

### Keywords:

Focused ultrasound

Brain

Drug delivery

Glioma

Blood–brain barrier

Chemotherapy

## ABSTRACT

The blood–brain–barrier (BBB) prevents the transport of most anticancer agents to the central nervous system and restricts delivery to infiltrating brain tumors. The heterogeneous vascular permeability in tumor vessels, along with several other factors, creates additional barriers for drug treatment of brain tumors. Focused ultrasound (FUS), when combined with circulating microbubbles, is an emerging noninvasive method to temporarily permeabilize the BBB and the “blood–tumor barrier”. Here, we tested the impact of three weekly sessions of FUS and liposomal doxorubicin (DOX) in 9L rat glioma tumors. Animals that received FUS + DOX (N = 8) had a median survival time that was increased significantly (P < 0.001) compared to animals who received DOX only (N = 6), FUS only (N = 8), or no treatment (N = 7). Median survival for animals that received FUS + DOX was increased by 100% relative to untreated controls, whereas animals who received DOX alone had only a 16% improvement. Animals who received only FUS showed no improvement. No tumor cells were found in histology in 4/8 animals in the FUS + DOX group, and in two animals, only a few tumor cells were detected. Adverse events in the treatment group included skin toxicity, impaired activity, damage to surrounding brain tissue, and tissue loss at the tumor site. In one animal, intratumoral hemorrhage was observed. These events are largely consistent with known side effects of doxorubicin and with an extensive tumor burden. Overall this work demonstrates that multiple sessions using this FUS technique to enhance the delivery of liposomal doxorubicin have a pronounced therapeutic effect in this rat glioma model.

© 2013 Elsevier B.V. All rights reserved.

## 1. Introduction

The blood–brain barrier (BBB) and other challenges prevent the effective use of most systemically-administered chemotherapeutic agents in patients with brain tumors. The BBB restricts transport of practically all agents to the brain parenchyma due to its selective permeability, which is based on lipid solubility, molecular size and charge [1,2]. Infiltrating tumor cells and metastatic “seeds” in the central nervous system are protected by the intact BBB and are excluded from the therapeutic effects of most drugs. Tumor blood vessels, which often lack an intact BBB, will allow some agent to extravasate and reach the vascular portion of the tumor. However, the permeability of the tumor vasculature is heterogeneous, and factors such as increased interstitial pressure [3] limit how far from the vasculature the drugs can penetrate. Furthermore, efflux pumps, which are present at

the BBB and in many tumors, extrude cytotoxic drugs that usually enter cells by passive diffusion [4]. Methods to overcome these barriers to drug delivery are needed if effective brain tumor therapies are to be developed.

Because of these challenges, the treatment of glioblastoma multiforme (GBM), an aggressive, high-grade brain tumor, is difficult [5]. This tumor is highly infiltrative, and recurrence after localized treatments such as conformal radiotherapy or surgery is common. This relapse usually occurs within a few cm of the treated region [6–8]. The introduction of temozolomide, a small molecule chemotherapy agent that has some penetration across the BBB, has improved clinical outcomes [9], but this improvement has been modest. A technique that can deliver larger agents across the “blood–tumor barrier” (BTB) and the BBB in the surrounding brain could enable the use of a wide range of anticancer agents for GBM and other brain tumors.

The use of focused ultrasound (FUS) combined with a circulating microbubble agent is an emerging technique to disrupt the BBB temporarily in a localized and non-invasive manner [10]. The microbubbles, which are constrained to the vasculature, interact strongly with even low-intensity ultrasound, producing mechanical forces on the endothelium that result in transient disassembly of tight junctional complexes

<sup>☆</sup> Conflict of interest: The last author holds two patents on the ultrasound technique evaluated in this work. The other authors have no conflicts of interest to report.

\* Corresponding author at: 221 Longwood Avenue, Boston, MA 02115, USA. Tel.: +1 617 732 5920; fax: +1 617 525 7450.

E-mail address: [muna@bwh.harvard.edu](mailto:muna@bwh.harvard.edu) (M. Aryal).

and the induction of active transport processes [11,12]. No significant adverse effects have been observed resulting from this temporary BBB disruption [13–15]. The barrier is restored in a few hours [10], providing a time-window to deliver even long-circulating agents. Prior work in animals has demonstrated delivery of a wide range of imaging and therapeutic agents, even large agents such as antibodies, nanoparticles, and liposomally-encapsulated drugs [16–19]. The method can increase the delivery of agents to brain tumors [20,21], and several studies have shown that it can improve outcomes in animal brain tumor models [20,22–24]. These results, along with recent work demonstrating safety in a large animal model using a clinical brain FUS system [13] make it a promising approach for the treatment of GBM and other brain tumors. Volumetric BBB disruption can be achieved with such devices by rapidly steering the ultrasound focal point to different locations [13].

This method has several potential advantages over other approaches tested to overcome the BBB and the BTB [25]. FUS-induced BBB disruption is a noninvasive and targeted procedure, and the effect can be localized to only desired volumes in the brain. The method is also compatible with currently-available drugs, removing the need to develop new agents. Importantly, since FUS is noninvasive and can presumably be applied without general anesthesia, it is expected to be a relatively benign procedure that can be readily repeated to match a patient's drug schedule.

The purpose of this work was to evaluate whether multiple treatment sessions can effectively improve the therapeutic effect of liposomal doxorubicin in a rat glioma model. Previous work has shown that a single treatment with FUS-enhanced delivery of this agent to orthotopically-implanted 9L rat gliosarcoma model had a modest improvement in survival and tumor growth [24]. Here we examined whether three weekly sessions can provide a more pronounced treatment effect in this tumor model. We also utilized low-frequency FUS to better match an existing clinical FUS device [26].

## 2. Materials and methods

### 2.1. Sonication system

An air-backed, single element, 690 kHz focused piezoelectric transducer (diameter/radius of curvature: 100/80 mm) generated the ultrasound field. It was driven by an arbitrary waveform generator (model 395, Wavetek) and RF amplifier (240L, ENI); electric power was measured with a power meter (E4419B, Agilent) and a dual-directional coupler (C5948-10, Werlatone). Reported exposure levels are absolute peak negative pressure amplitudes measured in water with a membrane hydrophone (Marconi; 0.5 mm diameter). Attenuation by the brain and rat skull is expected to reduce the pressure amplitude by ~30% at this frequency [27] with additional uncertainty arising from standing waves within the skull and increases in skull thickness as the animal ages [27]. The pressure distribution of the transducer was mapped using a 0.2 mm needle hydrophone (Onda, Sunnyvale, CA); its half-maximum diameter and length were 2.3 and 12 mm, respectively. The transducer efficiency was measured using a radiation force-balance.

### 2.2. Experimental setup

The sonication system was operated within a clinical 3 T MRI scanner (Signa; GE Healthcare). The transducer was immersed in a small tank of degassed, deionized water and attached to an MRI-compatible, manually-operated positioning system (Fig. 1A). The animal was laid supine on a tray above this tank, with a water bag providing an acoustic path to the dorsal surface of the head. Images were obtained with a 7.5 cm-diameter transmit/receive MRI surface coil. The animal's body temperature was maintained with a heated water pad. Before treatment, we visualized heating in a silicone phantom using temperature-sensitive MRI to localize the acoustic focal point in the MRI space.

Accurate targeting *in vivo* was confirmed before the tumor sonications in select animals (typically the first animal treated each week) by sonicating a spot in the brain outside the tumor and checking that the resulting MRI contrast extravasation was at the desired target.

### 2.3. Animals

The experiments were approved by our institutional animal committee. Tests were performed in 40 male Sprague–Dawley rats (Charles River Laboratories; ~250 g). Before each procedure, the animals were anesthetized *via* intraperitoneal injections of Ketamine (80 ml/kg/h) and Xylazine (10 ml/kg/h). A catheter was placed in the tail vein, and the hair on the scalp was removed with clippers and depilatory cream.

9L rat gliosarcoma cells (passage number 3, obtained from the Neurosurgery Tissue Bank at UCSF) were grown in Minimum Essential Medium (1×) with Earle's salts, supplemented with 10% fetal bovine serum, 1% L-glutamine, 1% MEM nonessential amino acids, and 0.1% gentamicin in a 5% CO<sub>2</sub> chamber held at 37 °C. After preparing the skin, a 5-mm skin incision was made and a 1-mm burr hole was drilled into the skull 1 mm anterior to the bregma and 2 mm lateral to the midline. A 4 µl volume of cell suspension (1 × 10<sup>5</sup> cells) was injected into the right caudate putamen at a depth of 3.5 mm relative to the dural surface using a 10 µl gas-tight syringe (Hamilton). Cells were injected over five minutes; two minutes later the needle was retracted slowly over another 5 min, and the skin was sutured. The sutures were removed 5 days later, and treatment began on day 7 or 8, at which point the tumor had an MRI-evident diameter between 1 and 3 mm.

The animals were monitored regularly to evaluate the treatment effects on survival and tumor growth. Animals surviving 6 weeks after treatment were considered long-term survivors. However, some were followed for longer periods for later histological examination, as they appeared healthy. The animals were euthanized if they exhibited severely impaired activity, weight loss exceeding 20% within one week, tumor dimensions exceeding 10–11 mm, or if treatment-related severe adverse events occurred that caused pain or distress and that could not be ameliorated. The animals were euthanized *via* transcardial perfusion with saline followed by 10% phosphate-buffered formalin while under deep anesthesia. The brain was removed and immersed in 10% phosphate-buffered formalin for histological preparation. To avoid skin infections that were observed in two animals (see below), animals receiving FUS and chemotherapy were treated with an antibiotic Baytril (Bayer; 2.5 mg/kg).

### 2.4. Treatment

The rats were randomly assigned to one of four groups: (1) no treatment (Control) (N = 7), (2) three weekly treatments with FUS-induced BBB/BTB permeabilization (FUS-Only) (N = 8), (3) three weekly treatments with liposomal doxorubicin (DOX-only) (N = 6), and (4) three weekly treatments with FUS and concurrent chemotherapy (FUS + DOX) (N = 8). After determining the coordinates of the focal point within the MRI space, treatment planning MRI was acquired, and the focal region was positioned within the tumor. Ultrasound bursts were then applied at multiple points in and around the tumor at pressure amplitudes ranging from 0.55 to 0.81 MPa (burst length: 10 ms, pulse repetition frequency: 1 Hz, duration: 60 s). The pressure amplitude was initially set based on a prior study in rats with this device [28]. It was increased based on the age and weight of the animals to achieve a consistent level of BBB disruption. This observation was made in our initial treatments and is similar to previous reports [27]. Before each sonication, ultrasonic contrast agent (DEFINITY, Lantheus Medical Imaging; 0.01 ml/kg) was administered intravenously. To facilitate the injections of such a small volume, the agent was diluted to 0.1× normal concentration in PBS. It was injected as a bolus

approximately 9 s before each sonication, followed by a 0.2 ml saline flush. The sonications were delivered at 5 min intervals in a grid pattern (spacing: 1 or 1.5 mm, depending on tumor volume) to 5–20 targets with the number of locations increasing over the three weeks as the tumor volume increased. We aimed to permeabilize the BTB in the entire tumor and the BBB in a surrounding rim of at least 1 mm.

For chemotherapy, 5.67 mg/kg of doxorubicin hydrochloride encapsulated in long-circulating pegylated liposomes was administered

intravenously. This dosage was selected based on prior work testing this agent in rats [29]. In our initial experiments (5 rats in DOX-Only group; 5 in FUS + DOX group), we used DOXIL (Centocor Ortho-Biotech). Due to a national shortage of this agent that occurred during these experiments, we used Lipo-DOX (TTY Biopharm) for the remaining animals (1 rat in the DOX-Only group; 3 in the FUS + DOX group). Previous work has shown that doxorubicin can be released from liposomes by ultrasound if microbubbles are in close vicinity [30], and we speculated that such may occur in these treatments. Thus for the FUS + DOX group, chemotherapy was administered over multiple slow injections administered just before each sonication. This scheme aimed to ensure a high drug concentration in the bloodstream during every sonication. For the DOX-only group, the agent was administered over 5 slow injections at 5 min intervals. Each injection was followed by a 0.2 ml saline flush.

## 2.5. Magnetic resonance imaging

T2-Weighted imaging was used to plan the treatments and measure tumor volumes. BBB/BTB disruption was evaluated using T1-weighted imaging acquired before and after administration of the MRI contrast agent gadopentate dimeglumine (Magnevist Gd-DTPA; Bayer Healthcare; 0.25 ml/kg). T2\*-Weighted imaging was used to confirm that petechiae, which are produced by excessive FUS exposures, did not occur [10] and to evaluate hemorrhagic regions in the tumors. Detailed imaging parameters are listed in Supplemental Methods.

## 2.6. Image analysis

Non-contrast MRI imaging was performed weekly ( $\pm 1$ –3 days depending on MRI availability). Tumor boundaries were manually segmented in axial T2-weighted images using ImageJ; the volume was calculated by the sum of the areas multiplied by the image thickness. In weeks 1–2, the tumors appeared as clearly circumscribed volumes which were sometimes surrounded by hyperintense regions (presumably edema). These boundaries were sometimes not evident at later times in the FUS + DOX group, and it was not clear whether MRI abnormalities were residual/recurring tumor or treatment-related effects. To be conservative, such cases were included in the volume calculations.

## 2.7. Histology

Representative examples from the Control (4/7 animals) and FUS-Only (5/8 animals) groups were selected for histological examination. The treatment response varied for animals in the DOX-Only and FUS + DOX groups (see below), and all brains from these animals were examined. Tissue blocks containing the tumor were embedded

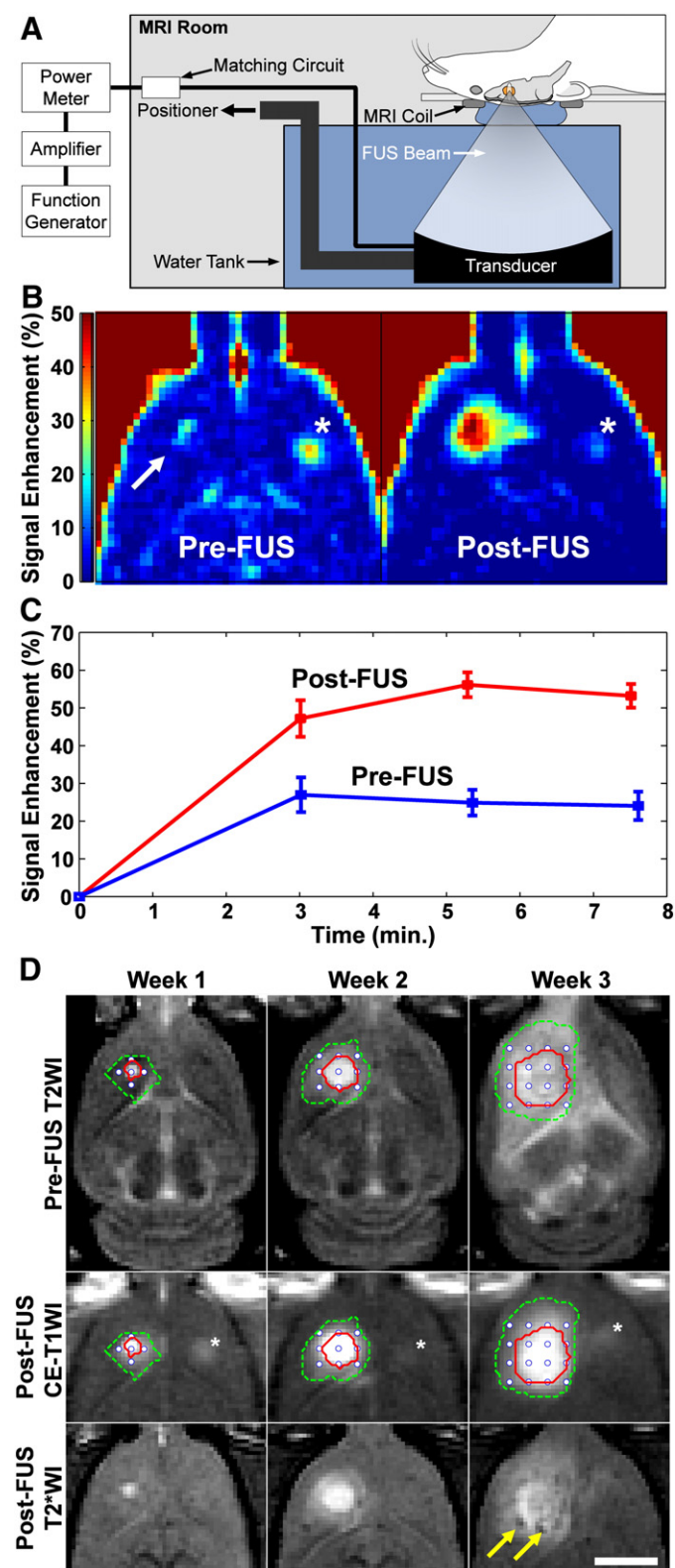
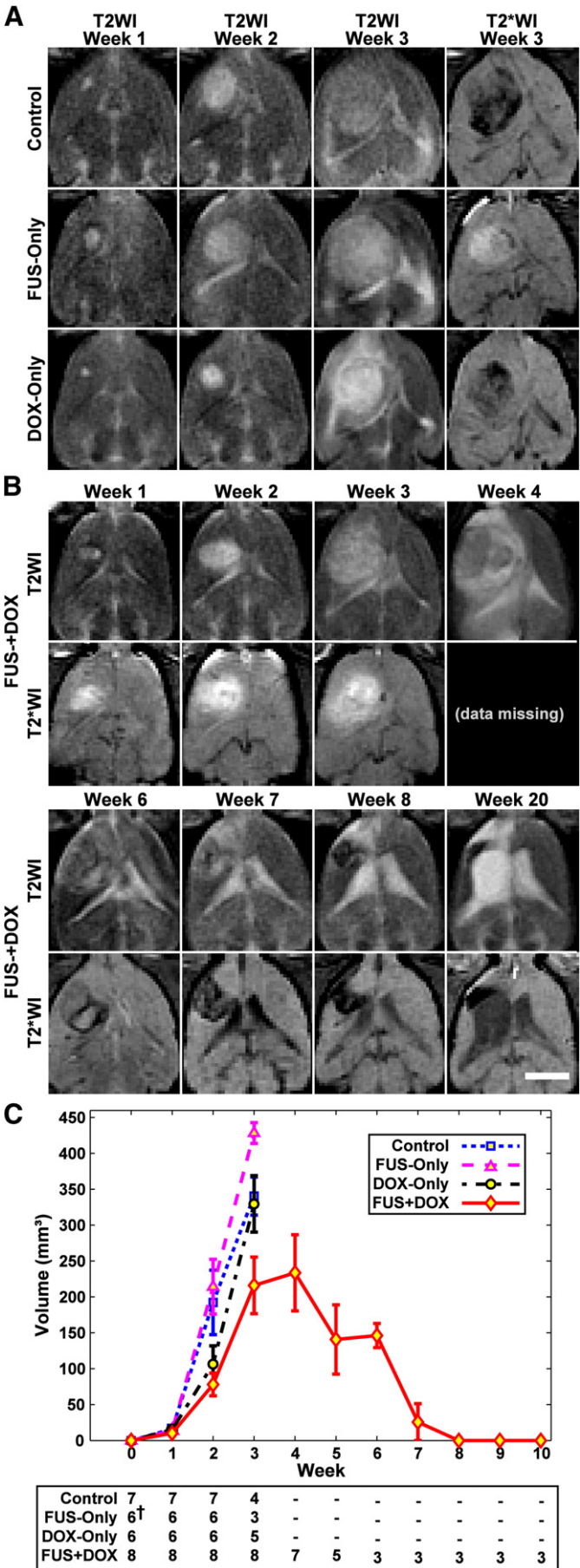


**Fig. 1.** Experimental setup and treatment overview. (A) Schematic of the MRI-guided focused ultrasound system used in this work. The function generator, amplifier, and power meter were located outside the MRI room (B). Axial images acquired before (left) and after (right) the first FUS + DOX treatment showing the signal enhancement in T1-weighted MRI after Gd-DTPA injection. Before FUS, the tumor was a small enhancing area (arrow). The magnitude and extent of this enhancement were increased after FUS. (C) Signal enhancement in this example as a function of time. (D) T2-weighted imaging (T2WI) used for treatment planning, contrast-enhanced T1-weighted imaging (CE-T1WI) used to verify the BBB/BTB permeabilization, and post-FUS T2\*-weighted imaging (T2\*WI) acquired during three weekly FUS + DOX treatments. (D) T2-weighted imaging (T2WI) used for treatment planning, contrast-enhanced T1-weighted imaging (CE-T1WI) used to verify the BBB/BTB permeabilization, and post-FUS T2\*-weighted imaging (T2\*WI). The location of the tumor in treatment planning is indicated by the solid line, and the extent of MRI contrast enhancement is indicated by the dotted line. The coordinates of the sonication targets are also noted (white circles). Two hypointense spots (arrows) were evident after the third treatment in T2\*-weighted imaging. The enhancing area evident in the other hemisphere in (B) and (D) (asterisk) was a location in the brain that was sonicated before the first Gd-DTPA injection to confirm the accurate targeting of the FUS beam. Bars: 5 mm.





in paraffin and cut into 4–6 μm serial sections perpendicular to the direction of ultrasound propagation. Sections with the largest evident tumor were stained with Hematoxylin and Eosin (H&E) for examination in light microscopy.

2.8. Statistical analysis

Tumor volumes for the four groups were compared using one-way ANOVA. The Kaplan–Meier method was used to compare survival of animals in each group. Significance was calculated by using log-rank test with Yates' correction. These analyses were performed using Matlab (MathWorks) and Microsoft Excel. The Bonferroni method was used to compare multiple pairs of groups [31]. With four treatment groups (including controls) and with six possible paired comparisons, pair-wise P values less than the Bonferroni-corrected threshold of  $0.05/6 = 0.0083$  were considered statistically significant.

3. Results

3.1. Tumor progression

BBB/BBT permeabilization and a lack of significant FUS-induced tissue damage were confirmed using contrast-enhanced and T2\*-weighted MRI, respectively (Fig. 1B). A higher pressure amplitude (0.81 vs. 0.55 MPa) was needed for the third treatment to induce consistent BBB/BBT permeabilization, presumably because of an increase in skull or dura thickness as the rats grew [27]. To confirm that the sonications increased the vascular permeability in the tumor, we performed contrast-enhanced imaging before and after the sonications in several animals (Fig. 1B–C). Sonication targets were applied in a grid to cover the tumor evident in T2-weighted imaging plus a surrounding margin (Fig. 1D). Weekly MRI examination was used to monitor the tumor progression. Representative examples from each experimental group over the first three weeks and the tumor volume measurements are shown in Fig. 2.

In most animals in the three control groups, the tumor grew rapidly over this time (Fig. 2A), resulting in significant midline shift and compression of the lateral ventricles. Hypointense regions were often evident within the tumor in T2\*-weighted imaging in all groups. Eleven of fifteen rats (73%) in these groups either died or were euthanized before the third treatment due either to tumor dimensions exceeding 10–11 mm or poor health conditions (weight loss exceeding 20% or severely impaired activity). The rest died or were euthanized for these reasons before week 4. One rat in the DOX-Only group was euthanized before the third treatment; the rest were euthanized shortly after week 3.

All animals in the FUS + DOX group received all three treatments, and no rat in this group was euthanized before week 4 (Fig. 2B–C). The tumor volume reached a maximum at weeks 3 or 4, after which

**Fig. 2.** MRI appearance of the tumors and their growth over time. (A) MRI for the three control groups for weeks 1–3. The rapid growth that was observed in most of the rats in these groups is evident in T2-weighted imaging (T2WI). Hypointense areas were often observed within the tumor in T2\*-weighted MRI (T2\*WI). (B) Serial MRI for a long-term survivor in the FUS + DOX group (Rat 4 in Table 1) showing rapid tumor growth and subsequent resolution. The volume was maximum at week four, at which time it covered a significant portion of one hemisphere. It then began to shrink, and from week 8 onwards it was no longer evident. Brain tissue loss at the former site was evident, and the lateral ventricle was enlarged and filled much of this space. Tissue adjacent to the former tumor mass was highly hyperintense in T2-weighted imaging, and presumably damaged. A hypointense region was observed at the former tumor site in T2\*-weighted imaging starting at weeks 6–7, which slowly shrunk over time. Imaging between weeks 8 and 20 was mostly similar. Note that the T2\*-weighted imaging in the FUS-Only and FUS + DOX animals was acquired after Gd-DTPA in weeks 1–3; contrast enhancement was observed in the tumor and surrounding brain. Bar: 5 mm. (C) MRI-measured tumor volumes as a function of time for each experimental group. Tumors were implanted at week 0. The number of surviving animals at each week is noted below the plot (†MRI from two animals in the FUS-Only group was not included in this analysis due to poor image quality). Mean ± S.E. is shown.

they began to shrink. The outcomes for the eight animals in this group varied and are summarized in Table 2. The maximum tumor volume varied substantially, with some tumors reaching volumes similar to the control group, and others never reaching 100 mm<sup>3</sup>. The mean tumor volume in the FUS + DOX group was less than in the three control groups at weeks 2–3 (Fig. 2C). However the differences were not significant.

The first two rats treated in the FUS + DOX group (Rats 1 and 2 in Table 1) exhibited local skin toxicity (inflammation, peeling; minor bleeding) on the scalp and the front and hind paws beginning on or after week two. These two animals developed a skin infection and were euthanized at days 34 and 35. In their last imaging session, one of these animals had no tumor evident in MRI, and the other had a small tumor that appeared to be responding to the treatment. Subsequent animals were treated prophylactically with antibiotics. While skin irritation or mild inflammation was observed, they did not develop infections.

Three animals (Rats 3, 4 and 8 in Table 1) did not exhibit any evident morbidity. They gained weight and behaved normally. These animals were followed for 9 or more weeks, at which time they were euthanized for histological examination. One of these long-term survivors was euthanized at day 66; the other two were observed for longer periods (136 and 142 days). Tumors in these animals grew to a substantial volume (greater than 300 mm<sup>3</sup>) before they began to resolve. MRI from one of these animals is shown in Fig. 2B. After the tumors disappeared, brain tissue loss at the former tumor site was evident in MRI, along with damage in adjacent tissues and enlarged ventricles. Tissue damage appeared as highly hyperintense regions in T2-weighted imaging. In some regions, within this damaged area, discrete hyperintense zones in both T2\* and T2-weighted imaging were seen.

Two animals in the FUS + DOX group (Rats 5 and 7 in Table 1) were euthanized due to poor health at days 32 and 36, respectively. At the time of sacrifice, one of these animals exhibited only a small hyperintense region in T2-weighted imaging, and no tumor was evident in histology (see below). The other had an extensive hyperintense area in T2-weighted imaging, but only a small cluster containing a few tumor cells was found in histology. Finally, in one animal (Rat 6 in Table 1), a large hypointense region was observed in T2\*-weighted imaging at week 4 that was assumed to be intratumoral hemorrhage. This animal also exhibited impaired activity and was euthanized at this time.

### 3.2. Histological findings

Tumors in the Control and FUS-Only groups appeared at days 15–23 as solid masses that replaced large amounts of brain tissue (Fig. 3A). The tumor bulk consisted of viable and rapidly dividing spindle-shaped cells interspersed with multiple small necrotic sites.

**Table 1**  
Outcomes in FUS + DOX group.

Rat	Survival (days)	Maximum vol. in MRI (mm <sup>3</sup> )	Vol. in MRI at euthanasia (mm <sup>3</sup> )	Tumor found in histology	Outcome
1	34	244	63	Yes	Skin infection, euthanized
2	35	52	0	No	Skin infection, euthanized
3	66	358	0	No	Long-term survivor
4	142	365	0	No	Long-term survivor
5	32	424 <sup>2</sup>	424 <sup>2</sup>	Yes <sup>1</sup>	Poor health, euthanized
6	31	312	312	Yes	Intratumoral hemorrhage, euthanized
7	36	96	40	No	Poor health, euthanized
8	136	312	0	Yes <sup>1</sup>	Long-term survivor

<sup>1</sup> Only a small cluster containing a few tumor cells was found.

<sup>2</sup> A well-defined tumor margin was not evident in T2-weighted MRI at weeks 3–4 in this animal; only a large hyperintense region was observed (see Fig. 4F). The volume of this hyperintense region was included in the volume measurements, as we could not determine if this region was tumor or edema.

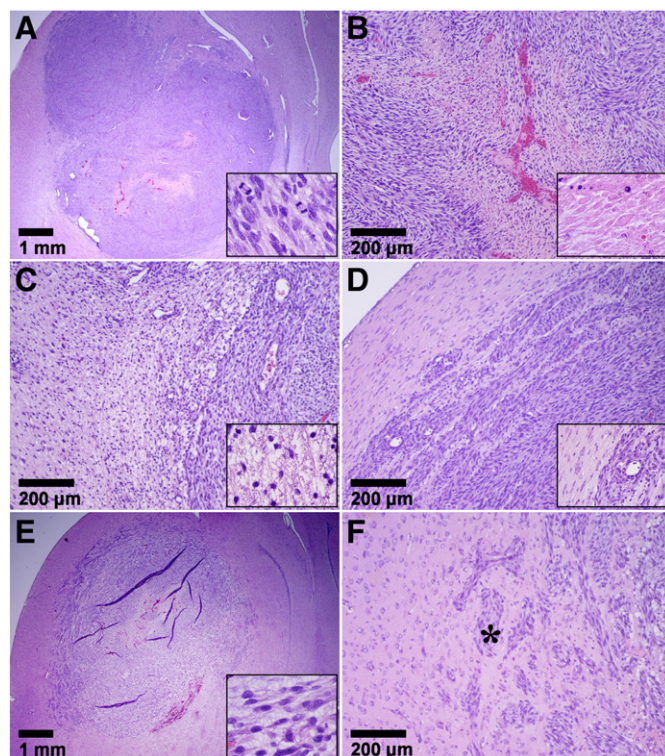


**Fig. 3.** Appearance of 9L gliosarcoma in the three control groups in histology. Animals receiving no treatment or FUS-Only (A–D) all had a similar appearance. The tumor appeared as a solid mass that replaced large volumes of brain tissue (A). The bulk of the tumors consisted of viable and rapidly dividing spindle-shaped cells (inset in A). Congested blood vessels were observed throughout, surrounded by necrotic tissue (B). Some regions of adjacent brain tissue were severely damaged, presumably from ischemia (C). There was a rim of infiltrating cells at the margin (D). Most tumors in the DOX-Only group (E–F) were also large masses of tumor cells with an infiltrating margin (E). However, unlike the other two control groups, they had a lower cellularity, unhealthy tumor cells, and intensely vacuolated matrix (inset in E). Tumor cell invasions along perivascular tracts and tumor cell clusters were observed at distant sites up to 2 mm from the edge of the solid tumor. The vacuolation evident in the tumor mass was often not observed in the infiltrating margin (\* in F).

Microvessels that were necrotic, dilated, and congested with erythrocytes were observed throughout and were surrounded by necrotic zones (Fig. 3B). Small hemorrhagic regions were also found. Blood cells in these regions and in congested blood vessels were consistent with the hypointense regions observed in T2\*-weighted imaging. In the largest tumors, numerous necrotic and hemorrhagic areas accompanied by cell necrosis and apoptosis were found scattered throughout the tumor mass. Rapid tumor growth and invasion displaced and compressed the surrounding brain tissue, resulting in ischemia and cell death (infarction) in some adjacent brain regions (Fig. 3C). A narrow (0.5–1 mm) band of invading/infiltrating cells was evident at the tumor margin (Fig. 3D).

The tumor appearance in the DOX-only group varied. Although viable and dividing cells were generally present, a reduced cellularity compared to the other control groups, along with unhealthy-appearing tumor cells and an intensely vacuolated matrix was evident in this group (Fig. 3E). Large regions of necrosis were observed in some cases, but some viable tumor cells were always found within these necrotic areas. Substantial hemorrhage was evident at the periphery of some tumors, accompanied by infarction in the surrounding brain. Tumor cell invasion along perivascular tracts and tumor cell clusters were observed at sites as far as 1–2 mm from the edge of the solid tumor mass (Fig. 3F). In one animal (euthanized at day 26 due to impaired activity), no tumor cells were found in histology.



In contrast to the controls, all but one of the animals in the FUS + DOX group exhibited a strong treatment response, with no tumor mass detected in 6/8 animals. However, in two of these animals a few residual or recurrent tumor cells were found in the former tumor site. In one rat, which was euthanized due to skin infection at day 34, a tumor was found to be shrunken compared to its maximum size in MRI and partly destroyed. The central area contained a viable tumor mass, and a surrounding rim of tissue appeared to be damaged. Only one animal (Rat 6 in Table 1) had a large tumor like most rats in the control groups. This animal, in which intratumoral bleeding was suspected in MRI, was euthanized at week 4. Histological examination confirmed hemorrhagic infarction in a region of tumor necrosis. This region was restricted to the tumor mass; no blood was found inside the adjacent ventricular space.

Example histological findings from the FUS + DOX group are shown in Fig. 4. In the three long-term survivors, where the tumors grew to a substantial volume before beginning to resolve, brain tissue loss was evident at the former tumor site (Fig. 4A). The adjacent lateral ventricle was significantly enlarged and filled this missing area. A region in the adjacent brain was necrotic, with an appearance consistent with infarct (Fig. 4B). A small cyst was observed within this necrotic zone. The hypointense regions evident in MRI contained hemosiderin – either in clusters or taken up by macrophages (inset in Fig. 4B). In one long-term survivor, a small cluster of recurring or residual tumor cells was found.

Findings from two animals from the FUS + DOX group that were euthanized for impaired activity are shown in Fig. 4C–H. In one case (euthanized at day 36) only a small necrotic area with macrophage infiltration was found at the former tumor site (Fig. 4C–E). In the second animal (euthanized at day 32), a larger necrotic area was found at the former tumor site, and affected or damaged tissue was observed in the surrounding brain that was hyperintense in T2-weighted MRI (Fig. 4F–H). A tiny cluster of tumor cells was found in this example (inset in Fig. 4G).

### 3.3. Survival analysis

Kaplan–Meier survival analysis is shown in Fig. 5; the corresponding statistical data are summarized in Table 2. The median survival time for the animals in both the Control and FUS-Only groups was about 18 days. For animals in the DOX-only group, it was 20.3 days – a 16% improvement over the animals in the Control group. However, this difference was not significant ( $P = 0.16$ ). In contrast, the animals in the FUS + DOX group showed a significant survival benefit ( $P < 0.001$ ) compared to the other three groups. The median survival time was 35 days, a 100% and 72% improvement over the Control and DOX-Only groups, respectively. Note that this analysis did not censor the two animals euthanized early due to skin infection. If one assumes those animals did not die from their tumor and censors them, the estimated median survival of the FUS + DOX group would be longer than 142 days, as more than 50% of the remaining animals survived until this time.

## 4. Discussion

Doxorubicin is a commonly-used anticancer drug for treatment of a wide range of cancers. While its effectiveness against glioma has been shown *in vitro* [32] and *in vivo* when injected directly into the tumor [33,34], systemic administration has not been effective clinically [35], presumably reflecting insufficient delivery [2]. A number of drug formulations have been developed to enhance the delivery of doxorubicin in animal glioma models [36–40] and at least one clinical trial is ongoing with such an agent [41]. Here, we demonstrated that ultrasound and microbubbles can effectively improve outcomes in a rat glioma model using an existing liposomal agent, removing

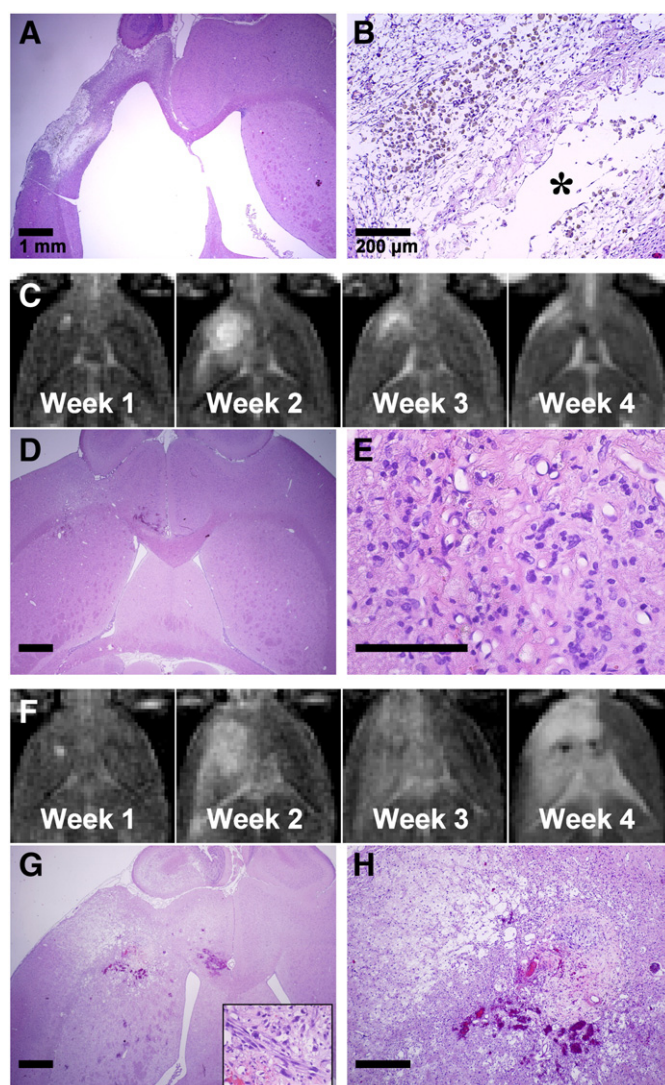


**Fig. 4.** Histological appearance of the brain in three of the animals from the FUS + DOX group. (A–B) Long-term survivor (see Fig. 2B for MRI). No tumor cells were found. Brain tissue loss at the former tumor site was evident, and the lateral ventricle was enlarged and filled this space. Tissue necrosis (infarct) was observed in the adjacent tissue, presumably from ischemia. Hemosiderin, either in clusters or inside macrophages was observed within the necrotic area. A small cyst (\*) was also observed. (C–E) Example from an animal, whose tumor was resolved, but the animal was euthanized at day 36 due to poor health. (C) T2-weighted MRI showing tumor growth and shrinkage. At week 4, only a small hyperintense region was visible. (D–E) A small necrotic area with macrophage infiltration was found at the former tumor site. (F–H) Another animal with a strong treatment response, but that was euthanized due to poor health at day 32. In this animal, the tumor grew to a relatively large size over weeks 1–2. At week 4, an extensive hyperintense area was observed in T2-weighted imaging (F). A necrotic area with micro-hemorrhages was found in histology at the former tumor site (G–H). Damaged or necrotic brain tissue was evident in the area that was hyperintense in T2-weighted imaging. A small cluster of tumor cells remained (inset in G).

the need to develop and test new drug formulations. The method is noninvasive and restricts the drug delivery only to desired brain regions. While more work is needed to optimize the treatment and to better understand its safety profile, these results are promising for the development of new treatment options for glioma patients. They join several other studies that showed this FUS method can enhance drug delivery and improve outcomes in brain tumor models [18,20–24,42].

This study also demonstrates the importance of multiple treatments. Previously, a modest survival improvement (24%) compared to untreated controls was observed with a single treatment in this tumor model [24]. With three weekly treatments, median survival

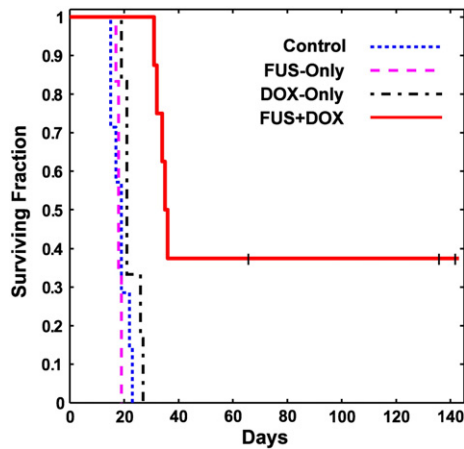


**Fig. 5.** Kaplan–Meier survival curves for the four experimental groups. Three long-term survivors, who did not exhibit impaired activity, were euthanized at different times (tick marks). Afterwards they were censored.

was increased by 100% compared to the controls, and we observed a 72% survival improvement compared to treatment with chemotherapy only. While the drug alone produced some treatment effects, it did not significantly improve survival or stop tumor proliferation in most cases. Histological examination of the tumors in this group showed a heterogeneous response to the treatment, with necrotic areas interspersed with viable tumor cells – perhaps consistent with heterogeneous vascular permeability and insufficient drug delivery to some regions. It also appeared that perhaps the drug did not reach the infiltrating tumor cells, as the matrix vacuolation evident in the tumor mass was not seen around the tumor cells at the tumor margin. In contrast, all but one of the tumors in the FUS + DOX group exhibited a strong treatment effect.

Several adverse events were observed. Three rats with little or no tumor evident in histology – one in the DOX-Only group and two in the FUS + DOX group – were euthanized due to impaired activity after three treatments. This finding may suggest that we used an aggressive treatment schedule that may not be tolerated by all subjects. Doxorubicin, even when encapsulated, has multiple known side effects, some of them severe. Use of medications to reduce the symptoms of these side effects may help to avoid the impairment we observed. In one animal (shown in Fig. 4F–H), damaged brain tissue was evident over a large portion of the treated hemisphere. We also observed brain tissue loss and necrosis in the surrounding brain in the three long-term survivors in the FUS + DOX group. We do not know whether these effects were due to the FUS + DOX treatment or to the extensive tumor burden that could have damaged the surrounding brain due to mass effects. While previous work did not find severe damage after one FUS + DOX treatment in normal rat brain [19], it is possible that cumulative effects from the three treatments, along with known neurotoxic effects of doxorubicin [43,44], produced this damage. If that is the case, attempting to aggressively

target infiltrating tumor cells with this agent may be contraindicated, and it may be necessary to either reduce the dosage delivered to the surrounding brain or to only target the vascular part of the tumor. Future work should evaluate the effects of multiple FUS + DOX treatments in the brain.

A potentially significant adverse event was the extensive intratumoral hemorrhagic area that occurred in one animal one week after the last FUS + DOX treatment. While we did not observe frank bleeding (such as into the ventricles), vascular risks associated the treatment should be examined in more detail. This hemorrhage may have resulted from necrosis of the vessel wall in a large tumor vessel. Others have reported hemorrhages in this tumor model with different doxorubicin formulations [40,45]. We also observed skin toxicity, a finding that may not be surprising since such toxicity, particularly in the hands and feet, is a known side effect of doxorubicin [46]. However, it might be prudent to confirm that the sonications do not increase drug delivery into the scalp. The focal region of our transducer overlapped the small rat skull, and the intensity on the scalp may have been relatively high. While the intensity on the scalp is expected to be less in humans, this issue might still be important, as large tumors may require sonication at hundreds of individual targets, and any low-level effects may accumulate. Reflections from the skull bone can exacerbate this effect.

This study had several limitations. First, due to a national shortage of DOXIL, we used a different drug formulation in some animals. While they had similar liposome properties, there may have been differences unknown to us that may have impacted our results. The sample size was also relatively small, and more work is needed to better characterize the effectiveness of the treatment and the rate of adverse events. More consistent results may be obtained using online methods to optimize the exposure levels. While we did modify the exposure levels based on the animal age and weight, we did not go back and re-treat regions where MRI contrast enhancement was poor to attempt to achieve a uniform level of enhancement. We anticipate that monitoring the microbubble dynamics in real-time using online acoustic emission monitoring [47,48] and re-treating areas with poor contrast enhancement can improve the local delivery and perhaps allow for a reduced systemic dose. Here, we evaluated only one dose of liposomal doxorubicin. We expect that by utilizing post-treatment MRI contrast imaging, which can be correlated to drug concentrations [19,49], along with online methods to control the exposures, we can optimize the drug dose delivered to the tumor and the surrounding brain tissue. Since liposomal doxorubicin has a long circulation time, we can sonicate regions where a higher dose is desired (such as the vascular portion of the tumor) repeatedly after a delay to extend the duration of BBB/BBB permeabilization [49] without increasing the dose to the surrounding brain tissue. It would also be interesting to investigate whether the sonications can release the doxorubicin from the liposomes, as has been observed by others with liposome-coated microbubbles [30].

Another limitation was our tumor model. While the 9L rat gliosarcoma model is highly aggressive and the robust survival improvement observed here is certainly encouraging, future work is needed with models that are genetically similar to human GBM and that have similar growth patterns. The 9L glioma model is not considered to be highly infiltrating [50] and we observed only a relatively narrow infiltrating zone. The disruption of the BBB in the surrounding brain tissue may not have played as large a role in our outcomes as might be anticipated clinically. Targeting infiltration is anticipated to be critically important with human GBM, and based on clinical patterns of recurrence [6–8], a margin extending several centimeters into the “normal” brain may require BBB disruption for effective therapy. Additional work in a more infiltrating tumor model is needed to ensure that we can safely and effectively target such regions. Finally, this model has been reported to be immunogenic [50], which may have led to more improved outcomes than would be achieved in non-immunogenic tumor model.

**Table 2**  
Survival analysis.

Treatment group	N animals	Max. survival (days)	Median survival (days)	IST <sub>median</sub> (%)	Mean survival ± S.D. (days)	P-Value, hazard ratio
Control	7	23	17.5	...	18.6 ± 3	...
FUS-Only	8	21	18.0	2.9	18.9 ± 1	0.85, 1.16
DOX-Only	6	27	20.3	16.2	22.5 ± 3	0.16, 1.18
FUS + DOX	8	>142	35.0	100.0	64.0 ± 48	0.00031, 5.36

Note – Increase in Survival Time [IST<sub>median</sub> (%)], P-value, and Hazard ratio are relative to the Control group.

P-Value and Hazard ratio from Log-Rank test between FUS + DOX and Dox-Only group are 0.00057 and 4.52 respectively.



Despite these limitations, the favorable outcome of these tests continues to support the development of this drug delivery technology for brain tumors and confirms the notion that a significant improvement in outcome can be achieved using multiple treatments. Going forward, we aim to validate these results in an infiltrating human GBM line and to integrate advanced methods for treatment planning, online monitoring, and post-treatment evaluation to maximize both the treatment efficacy and safety profile.

## 5. Conclusions

This work demonstrates that multiple sessions using this FUS technique to enhance the delivery of liposomal doxorubicin to tumors and the surrounding brain can have a pronounced therapeutic effect in this rat glioma model. A strong treatment effect was observed in 7/8 animals in our FUS + DOX group, with no tumor mass found in histology in six of the animals. Median survival was increased by 100% and 72% compared to control animals that received no treatment and DOX-Only, respectively. Adverse events, including damage to surrounding brain tissue, impaired activity, skin toxicity, and in one case, an extensively hemorrhagic tumor, were observed along with these treatment effects. While these events are consistent with known side effects of doxorubicin and with an extensive tumor burden, future work should be performed to examine the effects of multiple FUS + DOX sessions.

## Acknowledgments

This work was supported by NIH grants P41EB015898, P41RR019703, and R01EB003268 and from a gift from Brudnick family. We are grateful to Dr. Hao-Li Liu and Dr. Kuo-Chen Wei for supplying us with Lipo-Dox and Chanikarn Power for her technical help on the tumor implantation.

## Appendix A. Supplementary data

Supplementary data to this article can be found online at <http://dx.doi.org/10.1016/j.jconrel.2013.04.007>.

## References

- [1] W.M. Pardridge, Drug and gene delivery to the brain: the vascular route, *Neuron* 36 (4) (2002) 555–558.
- [2] H. von Holst, E. Knochenhauer, H. Blomgren, V.P. Collins, L. Ehn, M. Lindquist, G. Noren, C. Peterson, Uptake of adriamycin in tumour and surrounding brain tissue in patients with malignant gliomas, *Acta Neurochir. (Wien)* 104 (1–2) (1990) 13–16.
- [3] D. Fukumura, R.K. Jain, Tumor microenvironment abnormalities: causes, consequences, and strategies to normalize, *J. Cell. Biochem.* 101 (4) (2007) 937–949.
- [4] F.M. Kievit, F.Y. Wang, C. Fang, H. Mok, K. Wang, J.R. Silber, R.G. Ellenbogen, M. Zhang, Doxorubicin loaded iron oxide nanoparticles overcome multidrug resistance in cancer in vitro, *J. Control. Release* 152 (1) (2011) 76–83.
- [5] T.S. Surawicz, F. Davis, S. Freels, E.R. Laws Jr., H.R. Menck, Brain tumor survival: results from the National Cancer Data Base, *J. Neurooncol.* 40 (2) (1998) 151–160.
- [6] M.C. Chamberlain, Radiographic patterns of relapse in glioblastoma, *J. Neurooncol.* 101 (2) (2011) 319–323.
- [7] M.C. Dobelbower, O.L. Burnett Iii, R.A. Nordal, L.B. Nabors, J.M. Markert, M.D. Hyatt, J.B. Fiveash, Patterns of failure for glioblastoma multiforme following concurrent radiation and temozolomide, *J. Med. Imaging Radiat. Oncol.* 55 (1) (2011) 77–81.
- [8] G. Minniti, D. Amelio, M. Amichetti, M. Salvati, R. Muni, A. Bozzao, G. Lanzetta, S. Scarpino, A. Arcella, R.M. Enrici, Patterns of failure and comparison of different target volume delineations in patients with glioblastoma treated with conformal radiotherapy plus concomitant and adjuvant temozolomide, *Radiother. Oncol.* 97 (3) (2010) 377–381.
- [9] R. Stupp, M.E. Hegi, W.P. Mason, M.J. van den Bent, M.J. Taphoorn, R.C. Janzer, S.K. Ludwin, A. Allgeier, B. Fisher, K. Belanger, P. Hau, A.A. Brandes, J. Gijtenbeek, C. Marosi, C.J. Vecht, K. Mokhtari, P. Wesseling, S. Villa, E. Eisenhauer, T. Gorlia, M. Weller, D. Lacombe, J.G. Cairncross, R.O. Mirimanoff, Effects of radiotherapy with concomitant and adjuvant temozolomide versus radiotherapy alone on survival in glioblastoma in a randomised phase III study: 5-year analysis of the EORTC-NCIC trial, *Lancet Oncol.* 10 (5) (2009) 459–466.
- [10] K. Hynynen, N. McDannold, N. Vykhodtseva, F.A. Jolesz, Noninvasive MR imaging-guided focal opening of the blood–brain barrier in rabbits, *Radiology* 220 (3) (2001) 640–646.
- [11] X. Shang, P. Wang, Y. Liu, Z. Zhang, Y. Xue, Mechanism of low-frequency ultrasound in opening blood–tumor barrier by tight junction, *J. Mol. Neurosci.* 43 (3) (2011) 364–369.
- [12] N. Sheikov, N. McDannold, N. Vykhodtseva, F. Jolesz, K. Hynynen, Cellular mechanisms of the blood–brain barrier opening induced by ultrasound in presence of microbubbles, *Ultrasound Med. Biol.* 30 (7) (2004) 979–989.
- [13] N. McDannold, C. Arvanitis, N. Vykhodtseva, M. Livingstone, Temporary disruption of the blood–brain barrier by use of ultrasound and microbubbles: safety and efficacy evaluation in rhesus macaques, *Cancer Res.* 27 (2012) 3652–3663.
- [14] N. McDannold, N. Vykhodtseva, S. Raymond, F.A. Jolesz, K. Hynynen, MRI-guided targeted blood–brain barrier disruption with focused ultrasound: histological findings in rabbits, *Ultrasound Med. Biol.* 31 (11) (2005) 1527–1537.
- [15] Y.S. Tung, F. Vlachos, J.J. Choi, T. Deffieux, K. Selert, E.E. Konofagou, In vivo transcranial cavitation threshold detection during ultrasound-induced blood–brain barrier opening in mice, *Phys. Med. Biol.* 55 (20) (2010) 6141–6155.
- [16] J.F. Jordao, C.A. Ayala-Grosso, K. Markham, Y. Huang, R. Chopra, J. McLaurin, K. Hynynen, I. Aubert, Antibodies targeted to the brain with image-guided focused ultrasound reduces amyloid-beta plaque load in the TgCRND8 mouse model of Alzheimer's disease, *PLoS One* 5 (5) (2010) e10549.
- [17] M. Kinoshita, N. McDannold, F.A. Jolesz, K. Hynynen, Noninvasive localized delivery of Herceptin to the mouse brain by MRI-guided focused ultrasound-induced blood–brain barrier disruption, *Proc. Natl. Acad. Sci. U. S. A.* 103 (31) (2006) 11719–11723.
- [18] H.L. Liu, M.Y. Hua, H.W. Yang, C.Y. Huang, P.C. Chu, J.S. Wu, I.C. Tseng, J.J. Wang, T.C. Yen, P.Y. Chen, K.C. Wei, Magnetic resonance monitoring of focused ultrasound/magnetic nanoparticle targeting delivery of therapeutic agents to the brain, *Proc. Natl. Acad. Sci. U. S. A.* 107 (34) (2010) 15205–15210.
- [19] L.H. Treat, N. McDannold, N. Vykhodtseva, Y. Zhang, K. Tam, K. Hynynen, Targeted delivery of doxorubicin to the rat brain at therapeutic levels using MRI-guided focused ultrasound, *Int. J. Cancer* 121 (4) (2007) 901–907.
- [20] H.L. Liu, M.Y. Hua, P.Y. Chen, P.C. Chu, C.H. Pan, H.W. Yang, C.Y. Huang, J.J. Wang, T.C. Yen, K.C. Wei, Blood–brain barrier disruption with focused ultrasound enhances delivery of chemotherapeutic drugs for glioblastoma treatment, *Radiology* 255 (2) (2010) 415–425.
- [21] J. Mei, Y. Cheng, Y. Song, Y. Yang, F. Wang, Y. Liu, Z. Wang, Experimental study on targeted methotrexate delivery to the rabbit brain via magnetic resonance imaging-guided focused ultrasound, *J. Ultrasound Med.* 28 (7) (2009) 871–880.
- [22] P.Y. Chen, H.L. Liu, M.Y. Hua, H.W. Yang, C.Y. Huang, P.C. Chu, L.A. Lyu, I.C. Tseng, L.Y. Feng, H.C. Tsai, S.M. Chen, Y.J. Lu, J.J. Wang, T.C. Yen, Y.H. Ma, T. Wu, J.P. Chen, J.I. Chuang, J.W. Shin, C. Hsueh, K.C. Wei, Novel magnetic/ultrasound focusing system enhances nanoparticle drug delivery for glioma treatment, *Neuro Oncol.* 12 (10) (2010) 1050–1060.
- [23] E.J. Park, Y.Z. Zhang, N. Vykhodtseva, N. McDannold, Ultrasound-mediated blood–brain/blood–tumor barrier disruption improves outcomes with trastuzumab in a breast cancer brain metastasis model, *J. Control. Release* 163 (3) (2012) 277–284.
- [24] L.H. Treat, N. McDannold, Y. Zhang, N. Vykhodtseva, K. Hynynen, Improved anti-tumor effect of liposomal doxorubicin after targeted blood–brain barrier disruption by MRI-guided focused ultrasound in rat glioma, *Ultrasound Med. Biol.* 38 (10) (2012) 1716–1725.
- [25] W. Pardridge, Blood–brain barrier delivery, *Drug Discov. Today* 12 (2007) 54–61.
- [26] N. McDannold, G.T. Clement, P. Black, F. Jolesz, K. Hynynen, Transcranial magnetic resonance imaging-guided focused ultrasound surgery of brain tumors: initial findings in 3 patients, *Neurosurgery* 66 (2) (2010) 323–332, (discussion 332).
- [27] M.A. O'Reilly, A. Muller, K. Hynynen, Ultrasound insertion loss of rat parietal bone appears to be proportional to animal mass at submegahertz frequencies, *Ultrasound Med. Biol.* 37 (11) (2011) 1930–1937.
- [28] M. Pilatou, N. Vykhodtseva, N.J. McDannold, Blood–Brain Barrier Disruption in Rats Induced by Focused Ultrasound Under MRI Guidance: A Safety Study, MR-Guided Focused Ultrasound Symposium, Washington, DC, 2008.
- [29] Robert D. Arnold, Donald E. Mager, Jeanine E. Slack, Robert M. Straubinger, Effect of repetitive administration of doxorubicin-containing liposomes on plasma pharmacokinetics and drug biodistribution in a rat brain tumor model, *Clin. Cancer Res.* 11 (2005) 8856–8865.
- [30] B. Geers, I. Lentacker, N.N. Sanders, J. Demeester, S. Meairs, S.C. De Smedt, Self-assembled liposome-loaded microbubbles: the missing link for safe and efficient ultrasound triggered drug-delivery, *J. Control. Release* 152 (2) (2011) 249–256.
- [31] J.M. Bland, D.G. Altman, Multiple significance tests: the Bonferroni method, *BMJ* 310 (6973) (1995) 170.
- [32] A.C. Stan, S. Casares, D. Radu, G.F. Walter, T.D. Brumeau, Doxorubicin-induced cell death in highly invasive human gliomas, *Anticancer Res.* 19 (2A) (1999) 941–950.
- [33] K.A. Walter, R.J. Tamargo, A. Olivi, P.C. Burger, H. Brem, Intratumoral chemotherapy, *Neurosurgery* 37 (6) (1995) 1128–1145.
- [34] S. Voulgaris, M. Partheni, M. Karamouzis, P. Dimopoulos, N. Papadakis, H.P. Kalofonos, Intratumoral doxorubicin in patients with malignant brain gliomas, *Am. J. Clin. Oncol.* 25 (1) (2002) 60–64.
- [35] S. Ananda, A.K. Nowak, L. Cher, A. Dowling, C. Brown, J. Simes, M.A. Rosenthal, Phase 2 trial of temozolomide and pegylated liposomal doxorubicin in the treatment of patients with glioblastoma multiforme following concurrent radiotherapy and chemotherapy, *J. Clin. Neurosci.* 18 (11) (2011) 1444–1448.
- [36] T. Hekmatara, C. Bernreuther, A.S. Khalansky, A. Theisen, J. Weissenberger, J. Matschke, S. Gelperina, J. Kreuter, M. Glatzel, Efficient systemic therapy of rat glioblastoma by nanoparticle-bound doxorubicin is due to antiangiogenic effects, *Clin. Neuropathol.* 28 (3) (2009) 153–164.



- [37] T. Siegal, A. Horowitz, A. Gabizon, Doxorubicin encapsulated in sterically stabilized liposomes for the treatment of a brain tumor model: biodistribution and therapeutic efficacy, *J. Neurosurg.* 83 (6) (1995) 1029–1037.
- [38] S.C. Steiniger, J. Kreuter, A.S. Khalansky, I.N. Skidan, A.I. Bobruskin, Z.S. Smirnova, S.E. Severin, R. Uhl, M. Kock, K.D. Geiger, S.E. Gelperina, Chemotherapy of glioblastoma in rats using doxorubicin-loaded nanoparticles, *Int. J. Cancer* 109 (5) (2004) 759–767.
- [39] S. Wohlfart, A.S. Khalansky, C. Bernreuther, M. Michaelis, J. Cinatl Jr., M. Glatzel, J. Kreuter, Treatment of glioblastoma with poly(isohexyl cyanoacrylate) nanoparticles, *Int. J. Pharm.* 415 (1–2) (2011) 244–251.
- [40] R. Zhou, R. Mazurchuk, R.M. Straubinger, Antivasculature effects of doxorubicin-containing liposomes in an intracranial rat brain tumor model, *Cancer Res.* 62 (9) (2002) 2561–2566.
- [41] P. Gaillard, W. Gladdines, C. Appeldoorn, J. Rip, W. Boogerd, J. Beijnen, D. Brandsma, Olaf van Tellingen, Development of glutathione pegylated liposomal doxorubicin (2B3-101) for the treatment of brain cancer, *Cancer Res.* 72 (8) (2012).
- [42] F. Yang, M.-C. Teng, M. Lu, H.-F. Liang, Y.-R. Lee, C.-C. Yen, M.-L. Liang, T.-T. Wong, Treating glioblastoma multiforme with selective high-dose liposomal doxorubicin chemotherapy induced by repeated focused ultrasound, *Int. J. Nanomedicine* 7 (2012) 965–974.
- [43] E.A. Neuwelt, M. Glasberg, E. Frenkel, P. Barnett, Neurotoxicity of chemotherapeutic agents after blood–brain barrier modification: neuropathological studies, *Ann. Neurol.* 14 (3) (1983) 316–324.
- [44] A. Kondo, T. Inoue, H. Nagara, J. Tateishi, M. Fukui, Neurotoxicity of adriamycin passed through the transiently disrupted blood–brain barrier by mannitol in the rat brain, *Brain Res.* 412 (1) (1987) 73–83.
- [45] I. Brigger, J. Morizet, L. Laudani, G. Aubert, M. Appel, V. Velasco, M.J. Terrier-Lacombe, D. Desmaele, J. d'Angelo, P. Couvreur, G. Vassal, Negative preclinical results with stealth nanospheres-encapsulated doxorubicin in an orthotopic murine brain tumor model, *J. Control. Release* 100 (1) (2004) 29–40.
- [46] B. Uziely, S. Jeffers, R. Isacson, K. Kutsch, D. Wei-Tsao, Z. Yehoshua, E. Libson, F.M. Muggia, A. Gabizon, Liposomal doxorubicin: antitumor activity and unique toxicities during two complementary phase I studies, *J. Clin. Oncol.* 13 (7) (1995) 1777–1785.
- [47] N. McDannold, N. Vykhodtseva, K. Hynynen, Targeted disruption of the blood–brain barrier with focused ultrasound: association with cavitation activity, *Phys. Med. Biol.* 51 (4) (2006) 793–807.
- [48] M.A. O'Reilly, K. Hynynen, Blood–brain barrier: real-time feedback-controlled focused ultrasound disruption by using an acoustic emissions-based controller, *Radiology* 263 (1) (2012) 96–106.
- [49] J. Park, Y. Zhang, N. Vykhodtseva, F.A. Jolesz, N.J. McDannold, The kinetics of blood brain barrier permeability and targeted doxorubicin delivery into brain induced by focused ultrasound, *J. Control. Release* 162 (1) (2012) 134–142.
- [50] R.F. Barth, B. Kaur, Rat brain tumor models in experimental neuro-oncology: the C6, 9L, T9, RG2, F98, BT4C, RT-2 and CNS-1 gliomas, *J. Neurooncol.* 94 (3) (2009) 299–312.